Available online at www.sciencedirect.com
SCIENCE DIRECT®
Journal of Power Sources 126 (2004) 46–57
JOURNAL OF POWER SOURCES
www.elsevier.com/locate/jpowsour

Performance equations of polymer electrolyte fuel cells

Hsiao-Kuo Hsuen*
Department of Chemical Engineering, Yuan Ze University, Chung-Li 320, Taiwan, ROC

Received 22 July 2003; received in revised form 27 July 2003; accepted 30 August 2003

Abstract

Performance equations that describe the dependence of cell potential on current density for polymer electrolyte fuel cells (PEFCs) have been developed in algebraic form. The equations are derived from the reduction of a one-dimensional model that takes into account, in detail, the limitations of reactant transport, proton migration and electron conduction, as well as electrochemical reactions within the cathode, anode and membrane electrolyte. Reduction of the one-dimensional model is implemented by approximating the profiles of reactant concentration and ionomer potential with appropriate functions and by lumping the overall reaction rates at the reaction centres of the catalyst layers. Since the performance equations originate from a mechanistic one-dimensional model, all parameters appearing in the equations have a precise physical significance. In addition, individual potential losses caused by the various limiting processes can be clearly quantified in the equation. Particularly, the equations for potential losses relevant to the anode limiting processes are first revealed by the present work. Thus, they can be used as a diagnostic tool for PEFC performance. Computational results show that the performance equations agree well with the original one-dimensional model over an extensive parameter range. The present performance equations allow for an efficient evaluation of PEFC performance since the complexities of the one-dimensional model and the procedures for the numerical solutions are completely avoided. As compared with previously developed performance equations dealing with PEFC cathodes only, the present equations are able to provide accurate interpretation on the polarization behaviour of a complete PEFC.

Keywords: Polymer electrolyte; Fuel cell; Performance equation; Polarization; Modeling

1. Introduction

Fuel cells are power-generation devices that directly convert the chemical energy of fuels and oxygen into electricity through electrochemical reactions. Among all the various types of fuel cells, the polymer electrolyte fuel cell (PEFC) is the one characterized by using a proton-conductive membrane as its electrolyte layer. Due to the advantages of low emissions, low operating temperature, and short transient period to steady-state operation, PEFCs are promising candidates for primary power devices for electric vehicles. Up to the present stage, however, the commercialization of PEFCs is still restricted by prohibitively high cost. Reduction of the cost of PEFCs is achievable through the development of improved components for better performance, such as catalysts of high activity for the oxygen reduction reaction, membranes of low resistance for proton migration and gas diffusers with minimal water accumulation. On the other hand, mathematical modelling provides deeper insights into the transport and electrochemical processes taking place in PEFCs, and thus can be used as an efficient means for determining the most appropriate operating conditions and optimal design parameters.

Mechanistic models of PEFCs are formulated based on phenomenological transport, The kinetics of electrochemical reactions, and mass and energy conservation laws. Detailed consideration of the geometric configuration of PEFCs leads to two-dimensional and three-dimensional models [1–10]. In PEFCs, the cell thickness is orders of magnitude smaller than the other dimensions. Thus, although one-dimensional models are quite simple, they are still able to provide a good account of polarization characteristics under various operating current densities. A wide variety of one-dimensional models have been proposed [11–18].

The cell potential of a PEFC can be evaluated as the equilibrium value subtracted by the potential losses caused by the limitations of reactant transport, proton migration, electron conduction and electrochemical kinetics. Based on this observation, empirical models are formulated as a summation of a few terms that provide quantitative estimations of the equilibrium potential and the overpotentials pertinent to the related limiting processes. One of the simplest

* Tel.: +886-3-4638800x569; fax: +886-3-4559373.
E-mail address: skhsun@ce.yzu.edu.tw (H.-K. Hsuen).

0378-7753/$ – see front matter © 2003 Elsevier B.V. All rights reserved.
doi:10.1016/j.jpowsour.2003.08.040

Nomenclature

Notation

A_a, A_c	effective platinum surface area per unit volume ($cm^2\,cm^{-3}$)
b	dimensionless coordinate of anode-diffuser face
c_{H_2}	hydrogen concentration (mole cm^{-3})
d_a, d_c	gas-diffuser thickness (μm)
D^{eff}_{i-j}	effective binary diffusion coefficient for i and j species ($cm^2\,s^{-1}$)
$D^{eff}_{H_2}$	effective diffusivity of dissolved hydrogen in the catalyst layer ($cm^2\,s^{-1}$)
$D^{eff}_{O_2}$	effective diffusivity of dissolved oxygen in the catalyst layer ($cm^2\,s^{-1}$)
f_a, f_c	parameter (V^{-1}), f_a defined by Eq. (7c), $f_c = 4\alpha_c F/RT$
F	Faraday's constant (96487 C per equivalent)
H_{H_2}	Henry's constant for hydrogen (atm. cm^3 per mole)
H_{O_2}	Henry's constant for oxygen (atm. cm^3 per mole)
i^0_a, i^0_c	exchange current density at the reference condition ($A\,cm^{-2}$)
I	current density ($A\,cm^{-2}$)
I_a, I_c	characteristic current density ($A\,cm^{-2}$), I_a defined by Eq. (7f), $I_c = 4FP_c D^{eff}_{O_2}/H_{O_2}\delta_c$
$I_{lim,a}$	anode limiting current density ($A\,cm^{-2}$)
k^{eff}_a, k^{eff}_c	effective protonic conductivity for ionomer phase ($S\,cm^{-1}$)
k_m	protonic conductivity for membrane ($S\,cm^{-1}$)
N_i	mole flux of species i (mole $cm^{-2}\,s^{-1}$)
P_a, P_c	total pressure (atm.)
R	the universal gas constant (8.314 J per mol K)
r_1, r_2	ratio of diffusivities, defined by Eqs. (19a) and (19b)
T	temperature (K)
V	catalyst potential (V)
V_0	equilibrium potential of single cell (V)
V_a, V_c	potential of anode and cathode (V)
V^0_a, V^0_c	equilibrium potential of anode and cathode (V)
w	dimensionless position where hydrogen depletion occurs
x_i	mole fraction of species i
x^b_i	x_i in the bulk flow
$x^i_{H_2}$	x_{H_2} at the anode catalyst layer/membrane interface
$x^s_{H_2}$	x_{H_2} at the anode catalyst layer/anode-diffuser interface
$x^s_{O_2}$	x_{O_2} at the cathode catalyst layer/cathode-diffuser interface
z	coordinate perpendicular to the face of the anode diffuser (μm)

Greek letters

α_a, α_c	electrode transfer coefficient
β_a, β_c	parameter ($S\,cm^{-2}$), β_a defined by Eq. (7b), $\beta_c = k^{eff}_c/\delta_c$
β_m	parameter ($S\,cm^{-2}$), defined as k_m/δ_m
δ_a, δ_c	catalyst layer thickness (μm)
ε_a, ε_c	effective porosity of gas diffuser
ϕ	ionomer potential (V)
φ_a, φ_c	parameter, φ_a defined by Eq. (7a), $\varphi_c = A_c i^0_c H_{O_2}\delta^2_c/4FP_c D^{eff}_{O_2}$
σ^{eff}_a, σ^{eff}_c	effective electronic conductivity for gas diffuser ($S\,cm^{-1}$)
ζ	dimensionless coordinate, defined by Eq. (7e)

Subscripts

a	anode
c	cathode
m	membrane

is the model proposed by Srinivasan et al. [19], who suggested an equation for the conditions of activation and ohmic control. Such a simple equation is, however, not only unable to interpret experimental data at high current densities but is also incapable of elucidating the effects of most operating parameters. This equation was further modified by Kim et al. [20] through adding an exponential term to compensate for the potential loss at high current densities. Squadrito et al. [21] proposed an empirical equation, which includes a logarithmic function to account for the effects of mass-transport limitations. Since all these empirical equations are abundant with fitting coefficients, they can only be used as a data-fitting tool. Amphlett and his coworkers [22–24] derived the performance equations of PEFCs in a semi-empirical way, in which both mechanistic and fitting coefficients are present in the equations. Pisani et al. [25] presented a semi-empirical derivation of performance equations with the goal of having the largest number of mechanistic coefficients. Starting from a macro-homogeneous model for the cathode catalyst layer of PEFCs, Eikerling and Kornyshev [26] made efforts to formulate analytical expressions for the solutions of the model equations in order to rationalize the explicit effects of model parameters on cathode performance. Nevertheless, only solutions for a few limiting conditions were obtained.

In a previous work [27], a mechanistic approach was proposed to formulate the performance equations of PEFC cathodes. In this approach, the performance equations are

reduced from a one-dimensional model of PEFC cathodes by assuming appropriate profiles for oxygen concentration, ionomer and catalyst potentials. The derived performance equations are characterized in an explicit algebraic form as empirical models while keeping the same level of accuracy of the original one-dimensional model. In addition, all parameters appearing in the equations are endowed with a precise physical significance. Moreover, all contributive terms of potential losses caused by limiting transport processes and electrochemical kinetics can be quantitatively estimated. The previous performance equations only deal with the potential losses pertinent to the cathode of PEFCs. At medium and high current densities, the overpotentials associated with the anode and membrane electrolyte might also contribute significantly to the overall potential loss of PEFCs. Thus, it is also desirable to develop performance equations that include the potential losses of the cathode, anode and membrane electrolyte so as to elucidate the polarization behaviour of a complete PEFC. In order to achieve this goal, attention is first directed to the transport and electrochemical processes occurring within the PEFC anodes and equations for anode performance are formulated. The performance equations for a complete PEFC are then derived by combining the potential losses of its cathode, anode and membrane electrolyte. Because the accuracy of the cathode performance equations has been explored previously, it is only necessary to investigate the approximation errors of the anode. In addition, the characteristics of the performance equations of a single cell are discussed and the potential losses stemming from its cathode, anode and membrane electrolyte are analyzed.

2. One-dimensional model

The one-dimensional model considered in the present work is a steady-state and isothermal one. The present work extends the previous results for cathode performance to a single cell, which consists of a cathode, an anode and a membrane electrolyte. Except that the potential loss caused by electron conduction in the cathode catalyst layer is neglected, the assumptions employed previously for formulating the cathode model are also applied and will not be repeated here. Only the postulations concerning the anode and membrane electrolyte are listed below.

(i) The Stefan–Maxwell equations are employed for multi-component gas transport in the anode diffuser. It is assumed that a hydrogen-rich stream coming from methanol steam-reforming is used as an anode feed, which contains hydrogen, carbon dioxide and saturated water vapor. The effective binary gas diffusivity is described by the Bruggeman expression [12], which includes the effects of porosity and tortuosity.

(ii) Water vapour remains saturated within the gas diffuser and the mole flux of carbon dioxide is zero due to its inertness.

(iii) Catalyst particles and conductive ionomers are homogeneously mixed in the anode catalyst layer and the macro-homogeneous assumption is applied; it implies constant physical and chemical properties within the catalyst layer.

(iv) The hydrogen oxidation reaction follows the mechanism

$$H_2 + 2S \Leftrightarrow 2H\text{–}S \tag{1}$$

$$H\text{–}S \Leftrightarrow e^- + H^+ + S \tag{2}$$

where S denotes an active site on the catalyst surface. The above mechanism yields a half-order dependence of reaction rate on hydrogen concentration. The Butler–Volmer equation [28,29] is applied for the rate expression.

(v) Henry's law holds for the phase equilibrium of hydrogen at the interface between the anode diffuser and the anode catalyst layer.

(vi) The catalyst layer is nearly flooded and Fick's law is applied for the transport of dissolved hydrogen within it. The membrane is impermeable to dissolved hydrogen.

(vii) Potential loss due to electron conduction in the anode catalyst layer is considered to be negligible.

(viii) The membrane is fully hydrated and its ionic conductivity is a constant.

Based on the assumptions stated above, the equations based on mass conservation, electro-neutrality and Ohm's law can be expressed in partially dimensionless form. In the anode gas diffuser ($1 < \zeta < b$):

$$\frac{P_a}{RT\delta_a}\frac{dx_{H_2}}{d\zeta} = -(1 - x_{w,a} - x_{H_2})N_{H_2} \times \left[\frac{1}{D^{eff}_{H_2-CO_2}} + \frac{x_{w,a}}{x_{H_2}D^{eff}_{w-CO_2} + (1-x_{w,a}-x_{H_2})D^{eff}_{H_2-w}}\right] \tag{3}$$

$$\frac{dN_{H_2}}{d\zeta} = 0 \tag{4}$$

In the anode catalyst layer ($0 < \zeta < 1$):

$$\frac{d^2x_{H_2}}{d\zeta^2} + \varphi_a\{\exp[f_a(V_a^0 - V + \phi)] - \exp[-f_a(V_a^0 - V + \phi)]\}x_{H_2}^{1/2} = 0 \tag{5}$$

$$\frac{d^2x_{H_2}}{d\zeta^2} + \frac{\beta_a}{I_a}\frac{d^2\phi}{d\zeta^2} = 0 \tag{6}$$

The model parameters appearing in the above expressions are defined by:

$$\varphi_a = \frac{A_a i_a^0 H_{H_2}\delta_a^2}{2FP_a D^{eff}_{H_2}} \tag{7a}$$

$$\beta_a = \frac{k_a^{eff}}{\delta_a} \tag{7b}$$

$$f_a = \frac{\alpha_a F}{RT} \tag{7c}$$

$$\zeta = \frac{z}{\delta_a} \tag{7d}$$

$$x_{H_2} = \frac{H_{H_2} c_{H_2}}{P_a} \tag{7e}$$

$$I_a = \frac{2FP_a D_{H_2}^{eff}}{H_{H_2}\delta_a} \tag{7f}$$

where D_{i-j}^{eff} is an effective binary diffusivity in the porous medium for i and j species; N_i the mole flux of species i; x_i the mole fraction; α_a the anode transfer coefficient; A_a the effective platinum surface area per unit volume; i_a^0 the anode exchange current density at the reference condition; T the temperature; R the universal gas constant; P_a the anode pressure; c_{H_2} the dissolved hydrogen concentration; V_a^0 the anode equilibrium potential; V is the catalyst potential; ϕ is the ionomer potential; δ_a is the thickness of the anode catalyst-layer; H_{H_2} is the Henry's constant for gaseous hydrogen and its dissolved form in the ionomer phase. In the above expressions, x_{H_2} stands for the hydrogen mole fraction in the gas phase of the diffuser but represents the dimensionless concentration of dissolved hydrogen in the ionomer phase within the anode catalyst layer, as defined by Eq. (7e). The same symbol is used in both regions because, by such definitions, the x_{H_2} profiles are continuous across their boundary. It is also assumed that the transfer coefficients for anodic and cathodic reactions at the anode are equal; they are denoted as α_a in the above equations.

At the anode diffuser face ($\zeta = b$), Eq. (4) is applied. Besides, the hydrogen mole fraction is equal to its value in the bulk flow. Therefore,

$$x_{H_2} = x_{H_2}^b \tag{8}$$

At the interface between the anode diffuser and the catalyst layer ($\zeta = 1$), in addition to Eq. (2), other conditions are written as

$$x_{H_2}(\text{catalyst layer}) = x_{H_2}(\text{gas diffuser}) \tag{9}$$

$$\frac{I_a}{2F}\frac{dx_{H_2}}{d\zeta}(\text{catalyst layer}) = -N_{H_2} \tag{10}$$

$$\frac{d\phi}{d\zeta} = 0 \tag{11}$$

The catalyst potential is related to the anode potential, denoted as V_a, by

$$V\,(\text{catalyst layer}) = V_a + \frac{2FN_{H_2}}{\lambda_a} \tag{12}$$

and

$$\lambda_a = \frac{\sigma_a^{eff}}{d_a} \tag{13}$$

where σ_a^{eff} is the effective electric conductivity of the anode diffuser and d_a is its thickness. At the interface between the membrane and the anode catalyst-layer ($\zeta = 0$), the boundary conditions are formulated as

$$\phi = 0 \tag{14}$$

$$\frac{dx_{H_2}}{d\zeta} = 0 \tag{15}$$

The cathode equations are similar to those of the anode. Details have been presented elsewhere [27].

The method of collocation on finite elements based on cubic B-spline interpolation was employed for the solutions of the model equations [30]. The equations of anode and cathode were solved separately. First, the cathode equations were iterated with a fixed cathode potential. After a solution was obtained, the current density was evaluated, which was then employed and fixed during the iterations of the anode equations. The details of numerical procedures can be found in the previous work [27]. The output potential of a single cell was calculated as its equilibrium value deducted by the potential losses of its anode, cathode and membrane electrolyte.

3. Anode performance equations

It is assumed that the dimensionless hydrogen concentration profile within the anode catalyst layer be approximated by:

$$x_{H_2} = \{[(x_{H_2}^s)^{1/2} - (x_{H_2}^i)^{1/2}]\zeta^2 + (x_{H_2}^i)^{1/2}\}^2 \tag{16}$$

Where $x_{H_2}^s$ represents the value of x_{H_2} at the interface between the anode catalyst-layer and the anode diffuser, and $x_{H_2}^i$ is the value at the interface of the anode catalyst-layer and the membrane. Eq. (16) automatically satisfies the boundary conditions required by the x_{H_2} profile at $\zeta = 0$ and 1. Because the current density is equivalent to the flux of dissolved hydrogen at the interface between the anode catalyst-layer and the anode diffuser multiplied by $-2F$, $x_{H_2}^i$ can be expressed as:

$$x_{H_2}^i = \left[x_{H_2}^s - \frac{I}{4I_a}\right]^2 (x_{H_2}^s)^{-1} \tag{17}$$

where I stands for the current density. Eq. (1) can be solved analytically, thus one has

$$I = -2FN_{H_2} = -\frac{2FP_a D_{H_2-CO_2}^{eff}}{RTd_a} \times \ln\left(\frac{r_1 x_{H_2}^b + r_2 x_{CO_2}^b + x_{w,a}}{r_1 x_{H_2}^s + r_2 x_{CO_2}^s + x_{w,a}}\right)^{x_{w,a}/(x_{w,a}+r_1(1-x_{w,a}))} \times \left(\frac{x_{CO_2}^b}{x_{CO_2}^s}\right)^{r_1(1-x_{w,a})/(x_{w,a}+r_1(1-x_{w,a}))} \tag{18}$$

where:

$$r_1 = \frac{D^{\text{eff}}_{\text{CO}_2-\text{w}}}{D^{\text{eff}}_{\text{H}_2-\text{CO}_2}} \tag{19a}$$

$$r_2 = \frac{D^{\text{eff}}_{\text{H}_2-\text{w}}}{D^{\text{eff}}_{\text{H}_2-\text{CO}_2}} \tag{19b}$$

The anode limiting current ($I_{\text{lim,a}}$) can be obtained by setting $x^s_{\text{H}_2} = 0$ and $x^s_{\text{CO}_2} = 1 - x_{\text{w,a}}$ in Eq. (18). Similar to the cathode [27], an explicit approximation is used to calculate $x^s_{\text{H}_2}$ instead of Eq. (18), which has the form:

$$x^s_{\text{H}_2} = x^b_{\text{H}_2} - x^b_{\text{CO}_2}\left\{\left(\frac{x^b_{\text{H}_2}}{x^b_{\text{CO}_2}} + 1\right)^{I/I_{\text{lim,a}}} - 1\right\} \tag{20}$$

Eq. (20) provides a convenient means for evaluating $x^s_{\text{H}_2}$ since it skips the iterative procedures required by the original analytical solution. It yields exact values at $I = 0$ and $I_{\text{lim,a}}$ and also quite good accuracy for other intermediate values.

The rate of the hydrogen oxidation reaction is lumped at a reaction centre, which is defined by

$$\zeta^* = \frac{\int_0^1 \sqrt{x_{\text{H}_2}}\zeta \text{d}\zeta}{\int_0^1 \sqrt{x_{\text{H}_2}}\text{d}\zeta} = \frac{24x^s_{\text{H}_2}I_\text{a} - 3I}{48x^s_{\text{H}_2}I_\text{a} - 8I} \tag{21}$$

Based on this approximation, it is further postulated that the ionomer potential is flat from the interface between the anode diffuser and the anode catalyst-layer to the reaction centre due to the absence of proton migration. It decreases linearly from the reaction centre to the interface between the anode catalyst-layer and the membrane due to a constant protonic current. Therefore,

$$\phi = \frac{I\zeta}{\beta_\text{a}} \quad \text{for} \quad 0 < \zeta < \zeta^*; \quad \phi = \frac{I\zeta^*}{\beta_\text{a}} \quad \text{for} \quad \zeta^* < \zeta < 1 \tag{22}$$

According to the above approximations, the current density can be evaluated as:

$$I = \varphi_\text{a} I_\text{a}\{\exp[-f_\text{a}(V^0_\text{a} - V + \phi^*)] - \exp[f_\text{a}(V^0_\text{a} - V + \phi^*)]\}\bar{x}^{1/2}_{\text{H}_2} \tag{23}$$

where ϕ^* denotes the ionomer potential at the reaction center and $\bar{x}^{1/2}_{\text{H}_2}$ is defined as

$$\bar{x}^{1/2}_{\text{H}_2} = \int_0^1 x^{1/2}_{\text{H}_2}\,\text{d}\zeta = (x^s_{\text{H}_2})^{1/2} - \frac{1}{6}\frac{I}{I_\text{a}\sqrt{x^s_{\text{H}_2}}} \tag{24}$$

By inserting Eqs. (12), (22) and (24) into Eq. (23), the anode potential can be solved and expressed as

$$V_\text{a} = V^0_\text{a} + \left(\frac{24x^s_{\text{H}_2}I_\text{a} - 3I}{48x^s_{\text{H}_2}I_\text{a} - 8I}\right)\frac{I}{\beta_\text{a}} + \frac{I}{\lambda_\text{a}} + \frac{1}{f_\text{a}}\ln\left[\frac{3I\sqrt{x^s_{\text{H}_2}} + \sqrt{9I^2x^s_{\text{H}_2} + \varphi^2_\text{a}(6x^s_{\text{H}_2}I_\text{a} - I)^2}}{\varphi_\text{a}(6x^s_{\text{H}_2}I_\text{a} - I)}\right] \tag{25}$$

The overall potential loss in a PEFC anode is a linear combination of individual contributive terms stemming from the limitations of the involved transport processes and the electrochemical reaction, which include diffusion overpotential and ohmic loss for electron conduction within the anode diffuser, diffusion overpotential and ohmic loss for proton migration within the anode catalyst layer, and activation overpotential for the hydrogen oxidation reaction. Recall that the ohmic potential loss caused by electron conduction within the anode catalyst layer is not considered here due to its negligibly small value. The activation overpotential is referred to as the potential loss required to generate the required current density under the condition without any transport limitations and ohmic losses. Thus, the activation overpotential for the hydrogen oxidation reaction is

$$\frac{1}{f_\text{a}}\ln\left[\frac{I\sqrt{x^b_{\text{H}_2}} + \sqrt{I^2x^b_{\text{H}_2} + 4(\varphi_\text{a}x^b_{\text{H}_2}I_\text{a})^2}}{2\varphi_\text{a}x^b_{\text{H}_2}I_\text{a}}\right] \tag{26}$$

The ohmic loss caused by proton migration within the anode catalyst layer is estimated as the difference of ionomer potential at the interface between the membrane and the anode catalyst-layer and at the interface between the anode catalyst-layer and the anode diffuser, which has the form:

$$\text{ohmic loss (protonic) of anode catalyst layer} = \left(\frac{24x^s_{\text{H}_2}I_\text{a} - 3I}{48x^s_{\text{H}_2}I_\text{a} - 8I}\right)\frac{I}{\beta_\text{a}} \tag{27}$$

The diffusion overpotential of the anode diffuser arises from the decrease in hydrogen concentration from the diffuser face to the interface between the anode catalyst-layer and the anode diffuser, which is expressed as

$$\text{diffusion overpotential of anode diffuser} = \frac{1}{f_\text{a}}\ln\left[\frac{x^b_{\text{H}_2}(I\sqrt{x^s_{\text{H}_2}} + \sqrt{I^2x^s_{\text{H}_2} + 4(\varphi_\text{a}x^s_{\text{H}_2}I_\text{a})^2})}{x^s_{\text{H}_2}(I\sqrt{x^b_{\text{H}_2}} + \sqrt{I^2x^b_{\text{H}_2} + 4(\varphi_\text{a}x^b_{\text{H}_2}I_\text{a})^2})}\right] \tag{28}$$

The potential loss due to electron motion within the anode diffuser is determined by Ohm's law as

$$\text{ohmic loss (electronic) of anode diffuser} = \frac{I}{\lambda_\text{a}} \tag{29}$$

The diffusion overpotential of the anode catalyst layer reflects the potential loss caused by non-uniform distribution of hydrogen concentration inside the layer, which is evaluated as

$$\text{diffusion overpotential of anode catalyst layer} = \frac{1}{f_\text{a}}\ln\left[\frac{(2x^s_{\text{H}_2}I_\text{a})(3I\sqrt{x^s_{\text{H}_2}} + \sqrt{9I^2x^s_{\text{H}_2} + \varphi^2_\text{a}(6x^s_{\text{H}_2}I_\text{a} - I)^2})}{(6x^s_{\text{H}_2}I_\text{a} - I)(I\sqrt{x^s_{\text{H}_2}} + \sqrt{I^2x^s_{\text{H}_2} + 4(x^s_{\text{H}_2}\varphi_\text{a}I_\text{a})^2})}\right] \tag{30}$$

The applicability of Eq. (14) is limited to the condition:

$$x^b_{H_2} - x^b_{CO_2}\left\{\left(\frac{x^b_{H_2}}{x^b_{CO_2}}+1\right)^{I/I_{lim,a}} - 1\right\} - \frac{I}{4I_a} \geq 0 \qquad (31)$$

As Eq. (31) is violated, Eq. (16) is no longer applicable and Eq. (25) is not valid either. Under such a condition, it is proposed to employ a piecewise fourth-degree polynomial for the dimensionless hydrogen concentration profile within the anode catalyst layer, which is

$$x_{H_2} = x^s_{H_2}\left(\frac{\zeta - w}{1-w}\right)^4 \quad \text{for} \quad w \leq \zeta \leq 1 \quad \text{and}$$
$$x_{H_2} = 0 \quad \text{for} \quad 0 \leq \zeta \leq w \qquad (32)$$

where w is the dimensionless position in the anode catalyst layer where hydrogen depletion takes place. Relating the hydrogen transport rate at the interface of the anode catalyst-layer and the anode diffuser to the electric current density leads to

$$w = 1 - \frac{4x^s_{H_2} I_a}{I} \qquad (33)$$

Accordingly

$$\zeta^* = \frac{\int_w^1 \sqrt{x_{H_2}}\,\zeta\,d\zeta}{\int_w^1 \sqrt{x_{H_2}}\,d\zeta} = 1 - \frac{x^s_{H_2} I_a}{I} \qquad (34)$$

$$\bar{x}^{1/2}_{H_2} = \int_0^1 x^{1/2}_{H_2}\,d\zeta = \frac{4I_a (x^s_{H_2})^{3/2}}{3I} \qquad (35)$$

By following the same procedures, the anode potential can be expressed as

$$V_a = V^0_a + \left(1 - \frac{x^s_{H_2} I_a}{I}\right)\frac{I}{\beta_a} + \frac{I}{\lambda_a} + \frac{1}{f_a}\ln\left[\frac{3I^2 + \sqrt{9I^4 + 64\varphi^2_a I^4_a (x^s_{H_2})^3}}{8\varphi_a I^2_a (x^s_{H_2})^{3/2}}\right] \qquad (36)$$

The diffusion overpotential and the electronic ohmic loss of the anode diffuser and the activation overpotential for the hydrogen oxidation reaction have the same expressions as the previous condition. Other contributive terms have the forms

diffusion overpotential of anode catalyst layer

$$= \frac{1}{f_a}\ln\left[\frac{3I^2 + \sqrt{9I^4 + 64\varphi^2_a I^4_a (x^s_{H_2})^3}}{4I_a x^s_{H_2}\left(I + \sqrt{I^2 + 4\varphi^2_a I^2_a x^s_{H_2}}\right)}\right] \qquad (37)$$

ohmic loss (protonic) of anode catalyst layer

$$= \left(1 - \frac{x^s_{H_2} I_a}{I}\right)\frac{I}{\beta_a} \qquad (38)$$

4. Performance equations of a single cell

The output potential of a single cell can be estimated as the equilibrium potential deducted by the potential losses of its cathode, anode and membrane electrolyte. Based on the occurrence of depletion of oxygen and hydrogen in the catalyst layers of the cathode and the anode, four equations in different regimes are formulated contingent upon the sign of g and h, which are defined as:

$$g = x^b_{O_2} - x^b_{N_2} \times \left[\exp\left(\frac{RTd_c I}{4FP_c}\left[\frac{1}{D^{eff}_{N_2-O_2}} + \frac{x_{w,c}}{(1-x_{w,c})D^{eff}_{N_2-w}}\right]\right) - 1\right] - \frac{I}{2I_c} \qquad (39)$$

$$h = x^b_{H_2} - x^b_{CO_2}\left\{\left(\frac{x^b_{H_2}}{x^b_{CO_2}}+1\right)^{I/I_{lim,a}} - 1\right\} - \frac{I}{4I_a} \qquad (40)$$

For $g > 0$ and $h > 0$:

$$V_{cell} = V_0 - \frac{I}{\beta_c}\frac{(12x^s_{O_2} I_c - 3I)}{(24x^s_{O_2} I_c - 8I)} - \frac{I}{\lambda_c} - \frac{1}{f_c}\ln\left[\frac{I}{\varphi_c (x^s_{O_2} I_c - I/3)}\right] - \frac{I}{\beta_a}\left(\frac{24x^s_{H_2} I_a - 3I}{48x^s_{H_2} I_a - 8I}\right) - \frac{I}{\lambda_a} - \frac{1}{f_a}\ln\left[\frac{3I\sqrt{x^s_{H_2}} + \sqrt{9I^2 x^s_{H_2} + \varphi^2_a (6x^s_{H_2} I_a - I)^2}}{\varphi_a (6x^s_{H_2} I_a - I)}\right] - \frac{I}{\beta_m} \qquad (41)$$

For $g < 0$ and $h > 0$:

$$V_{cell} = V_0 - \frac{I}{\beta_c}\left(1 - \frac{x^s_{O_2} I_c}{2I}\right) - \frac{I}{\lambda_c} - \frac{1}{f_c}\ln\left[\frac{3I^2}{2\varphi_c (x^s_{O_2} I_c)^2}\right] - \frac{I}{\beta_a}\left(\frac{24x^s_{H_2} I_a - 3I}{48x^s_{H_2} I_a - 8I}\right) - \frac{I}{\lambda_a} - \frac{1}{f_a}\ln\left[\frac{3I\sqrt{x^s_{H_2}} + \sqrt{9I^2 x^s_{H_2} + \varphi^2_a (6x^s_{H_2} I_a - I)^2}}{\varphi_a (6x^s_{H_2} I_a - I)}\right] - \frac{I}{\beta_m} \qquad (42)$$

For $g < 0$ and $h < 0$:

$$V_{\text{cell}} = V_0 - \frac{I}{\beta_c}\left(1 - \frac{x^s_{O_2} I_c}{2I}\right) - \frac{I}{\lambda_c} - \frac{1}{f_c}\ln\left[\frac{3I^2}{2\varphi_c (x^s_{O_2} I_c)^2}\right] - \frac{I}{\beta_a}\left(1 - \frac{x^s_{H_2} I_a}{I}\right) - \frac{I}{\lambda_a} - \frac{1}{f_a}\ln\left[\frac{3I^2 + \sqrt{9I^4 + 64\varphi_a^2 I_a^4 (x^s_{H_2})^3}}{8\varphi_a I_a^2 (x^s_{H_2})^{3/2}}\right] - \frac{I}{\beta_m} \quad (43)$$

For $g > 0$ and $h < 0$

$$V_{\text{cell}} = V_0 - \frac{I}{\beta_c}\frac{(12 x^s_{O_2} I_c - 3I)}{(24 x^s_{O_2} I_c - 8I)} - \frac{I}{\lambda_c} - \frac{1}{f_c}\ln\left[\frac{I}{\varphi_c (x^s_{O_2} I_c - I/3)}\right] - \frac{I}{\beta_a}\left(1 - \frac{x^s_{H_2} I_a}{I}\right) - \frac{I}{\lambda_a} - \frac{1}{f_a}\ln\left[\frac{3I^2 + \sqrt{9I^4 + 64\varphi_a^2 I_a^4 (x^s_{H_2})^3}}{8\varphi_a I_a^2 (x^s_{H_2})^{3/2}}\right] - \frac{I}{\beta_m} \quad (44)$$

In the above expressions, the potential loss of the cathode was adopted from the results of the previous work [27]. The notions were modified so as to be consistent with the present work. It should be stated that the anodic reaction at the cathode is neglected in formulating the cathode performance equations. Nevertheless, both the anodic and cathodic reactions are taken into account in deriving the anode performance equations. Thus, it yields a more complex form than its counterpart for the cathode. Such an inclusion is compulsory to provide accurate estimations for anode performance due to a much higher value of the anode exchange current density. On the other hand, the impact of neglecting the anodic reaction at the cathode only appears in an extremely narrow region near the equilibrium potential.

5. Results and discussion

Because the accuracy of the performance equations for cathodes has been investigated in the previous study, this study first explores the differences between the results calculated based on the anode performance equations and the corresponding one-dimensional model and then discusses the features exhibited by the performance equations of single cells. Because the chemical and physical properties of PEFC anodes might vary by orders of magnitude with the materials, quantities and methods used for fabrication, the validity of the performance equations has to be tested over a wide range of parameter values. In order to do so, the parameter values listed in Table 1 were used as a base case for the anode, and computations were carried out by adjusting the magnitude of a particular parameter with other parameter values remaining fixed.

Table 1
Values of physical and chemical parameters for anode of the base case

Effective ionic conductivity of ionomer in anode, k_a^{eff} (S cm^{-1})	3×10^{-2}
Effective electric conductivity of anode gas diffuser, σ_a^{eff} (S cm^{-1})	0.5
Effective porosity of anode gas diffuser, ε_a	0.4
Effective diffusivity of dissolved hydrogen in the anode catalyst layer, $D^{\text{eff}}_{H_2}$ (cm^2 s^{-1})	8.4×10^{-7}
Effective gas-pair diffusivity, $D^{\text{eff}}_{H_2-CO_2}$ ($= \varepsilon_a^{1.5} D_{H_2-CO_2}$) (cm^2 s^{-1})	7.08×10^{-2}
Effective gas-pair diffusivity, $D^{\text{eff}}_{CO_2-w}$ ($= \varepsilon_a^{1.5} D_{CO_2-w}$) (cm^2 s^{-1})	2.11×10^{-2}
Effective gas-pair diffusivity, $D^{\text{eff}}_{H_2-w}$ ($= \varepsilon_a^{1.5} D_{H_2-w}$) (cm^2 s^{-1})	1.05×10^{-1}
Thickness of anode gas-diffuser, d_a (μm)	300
Thickness of anode catalyst-layer, δ_a (μm)	5
Product of platinum surface area and reference exchange current density of anode, $A_a i_a^0$ (A cm^{-3})	1.4×10^5
Anode pressure, P_a (atm.)	3
Temperature, T (K)	353
Bulk hydrogen mole fraction, $x^b_{H_2}$	0.633
Bulk carbon dioxide mole fraction, $x^b_{CO_2}$	0.211
Mole fraction of water vapor in anode, $x_{w,a}$	0.156
Henry's constant for hydrogen, H_{H_2} (atm. cm^3 per mole)	4.5×10^4
Equilibrium potential of anode, V_a^0 (V)	0
Anode transfer coefficient, α_a	0.5

The polarization curves calculated using the performance equations and the one-dimensional model for the base case are illustrated in Fig. 1. These two curves almost coincide. For the parameter values used in the calculations, the limiting current occurs around 54 A cm^{-2}, which is not included in Fig. 1 since such a value is far beyond the ones in practical operation. It appears that the anode potential

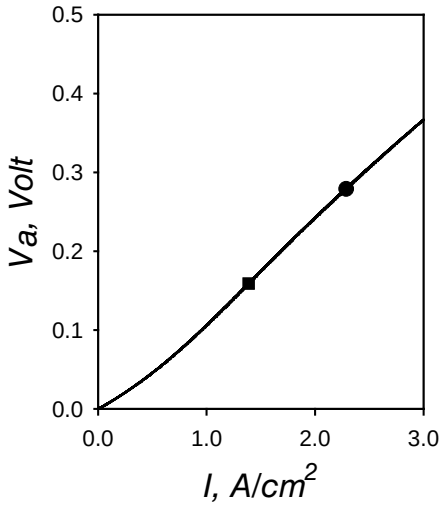

Fig. 1. Anode polarization curves for base case: (●) one-dimensional model; (■) performance equations.

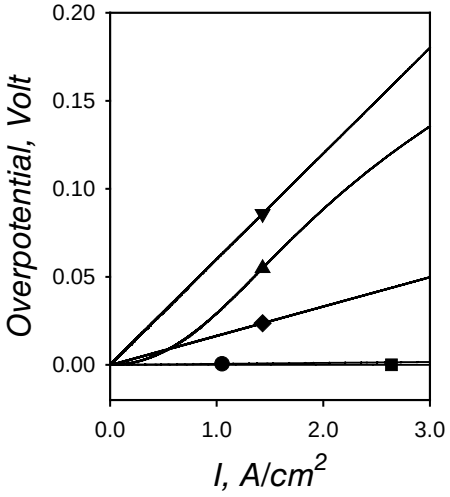

Fig. 2. Polarization curves of individual contributive terms for base case of anode calculated using performance equations: (■) activation overpotential; (▲) diffusion overpotential of catalyst layer; (●) diffusion overpotential of gas diffuser; (◆) ohmic potential loss of ionomer in catalyst layer; (▼) ohmic potential loss of gas diffuser.

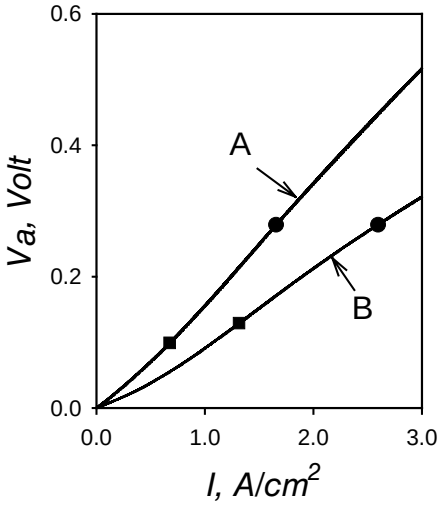

Fig. 3. Polarization curves for anodes with different catalyst-layer thickness. (A) $\delta_a = 20\,\mu m$; (B) $\delta_a = 0.5\,\mu m$; (●) one-dimensional model; (■) performance equations.

responds to current density in an approximately linear fashion for the calculated current range. Detailed analyses of the individual contributive terms of anode polarization are displayed in Fig. 2. It is seen that activation overpotential is almost negligible for the current range calculated. This fact is attributed to extremely fast reaction rates for hydrogen oxidation, exhibited by the product value of $A_a i_a^0$ listed in Table 1. The ohmic loss in the anode diffuser is linear with current density as revealed by Ohm's law. It is also seen that the ohmic loss caused by proton migration within the catalyst layer increases in a nearly linear manner with current density, although its expression in the performance equations involves complex forms of fractional and exponential functions. For the current range investigated in the present case, the diffusion overpotential of the anode diffuser is negligibly small due to relatively high values of gas-pair diffusivity of hydrogen and the effective porosity of the diffuser. Compared with other potential losses, the diffusion overpotential of the anode catalyst layer varies with current density in a more complex manner, which depends on the evolution of the hydrogen concentration profile within the layer.

Various techniques have been developed for the fabrication of catalyst layers so as to achieve an optimum structure, and hence improved performance. Owing to the different nature of fabrication methods, the thickness of an anode catalyst layer may vary by orders of magnitude. As a method of deposited sputtering is employed, a thickness of less than 1 μm is achievable [31]. The layer formed is much thicker, however, if it is prepared by printing with an ionomer/carbon-supported-platinum ink. In order to take such great discrepancies into account, two thicknesses with a wide variation were selected for the anode catalyst layer. The results are displayed in Fig. 3. As shown, the polarization curves obtained using the performance equations agree well with those from the one-dimensional model. A thicker catalyst layer implies that a larger space is available to accommodate the hydrogen oxidation reaction; thus, a lower activation overpotential is expected. For an extremely fast reaction like the present one, however, such an effect is not pronounced. On the other hand, a thicker catalyst layer imposes greater limitations for proton migration and hydrogen transport, which leads to a greater loss of anode potential. As illustrated, the anode with $\delta_a = 0.5\,\mu m$ exhibits better performance for one with $\delta_a = 20\,\mu m$ for entire range of current density calculated.

Investigation of the effects of $A_a i_a^0$ on the accuracy of the present anode performance equations was carried out for two anodes with different product values of $A_a i_a^0$, i.e. 1.4×10^6 and $1.4 \times 10^4\,A\,cm^{-3}$. The results are presented in Fig. 4. A rather good agreement is also found between the performance equations and the one-dimensional model, as in previous cases. In addition, a significant increase in the anode potential loss is observed for an electrode with $A_a i_a^0 = 1.4 \times 10^4\,A\,cm^{-3}$. In order to explore further the sources of such degradation, individual potential losses relevant to $A_a i_a^0$ were calculated based on the performance equations. The results are plotted in Fig. 5 and include the activation overpotential for the hydrogen oxidation reaction as well as the diffusion overpotentials of the diffuser and of the catalyst layer. It is seen that the diffusion overpotentials of the gas diffuser for these two cases are negligible and the activation overpotentials are only slightly different. Major degradation comes from the diffusion overpotential of the catalyst layer. Such results are quite different to those for cathodes, in which $A_c i_c^0$ only appears in the expression of activation overpotential and the diffusion overpotential of the catalyst layer does not rely on it. This dissimilarity stems from much higher values of anode exchange current

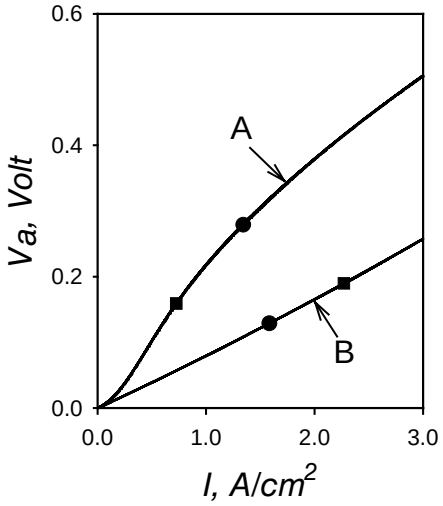

Fig. 4. Polarization curves for anodes with different product values of $A_a i_a^0$ (A) $A_a i_a^0 = 1.4 \times 10^4\,\mathrm{A\,cm^{-3}}$ (B) $A_a i_a^0 = 1.4 \times 10^6\,\mathrm{A\,cm^{-3}}$; (●) one-dimensional model; (■) performance equations.

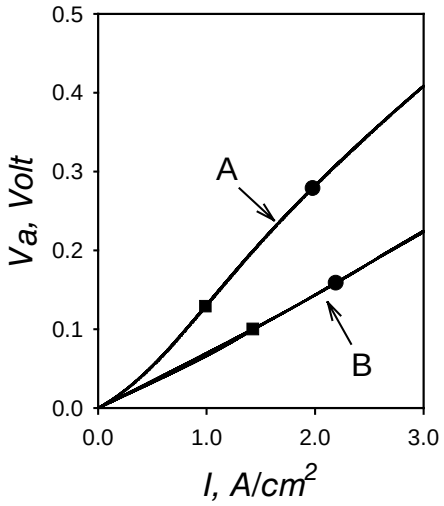

Fig. 6. Polarization curves for anodes with different values of effective hydrogen diffusivity in catalyst layer. (A) $D_{H_2}^{eff} = 4.2 \times 10^{-7}\,\mathrm{cm^2\,s^{-1}}$; (B) $D_{H_2}^{eff} = 4.2 \times 10^{-5}\,\mathrm{cm^2\,s^{-1}}$; (●) one-dimensional model; (■) performance equations.

density, which, in turn, lead to a substantial participation of the cathodic reaction at the anode.

Among all physical parameters involved in the performance equations, $D_{H_2}^{eff}$ is the only one that provides a quantitative measure for the transport ability of hydrogen under the multiphase configuration of the anode catalyst layer. Since the ionomers mixed in the catalyst layer are composed of hydrophobic backbone and hydrophilic groups, small amounts of gas pores might exist, which greatly facilitate hydrogen transport within the layer. Thus, the value of $D_{H_2}^{eff}$ may vary greatly from one anode to another due to different degrees of involvement of gaseous hydrogen transport within the anode catalyst layer. In order to cover such wide variations, two $D_{H_2}^{eff}$ values differing by a factor of 100, namely 4.2×10^{-7} and $4.2 \times 10^{-5}\,\mathrm{cm^2\,s^{-1}}$ were employed for calculations and the results are given in Fig. 6. As seen, quite good agreement is also found between the results from the performance equations and from the one-dimensional model. A higher $D_{H_2}^{eff}$ suggests that hydrogen is able to diffuse into the inner part of the catalyst layer and thus gives rise to increased catalyst utilization. Consequently, a lower potential is observed. Therefore, for the same current density, the anode with $D_{H_2}^{eff} = 4.2 \times 10^{-5}\,\mathrm{cm^2\,s^{-1}}$ always outperforms that with $D_{H_2}^{eff} = 4.2 \times 10^{-7}\,\mathrm{cm^2\,s^{-1}}$.

Polarization curves for two anodes with different values of effective ionomer conductivity in the anode catalyst layer are shown in Fig. 7. As illustrated, the polarization curves

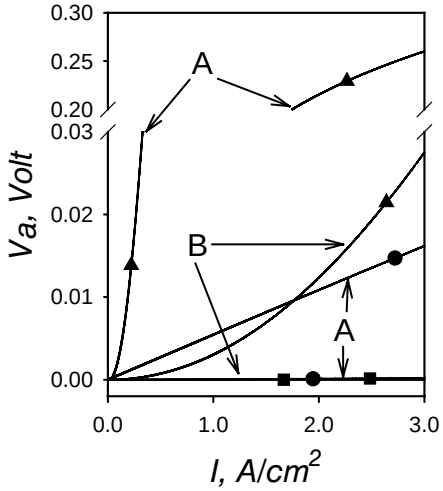

Fig. 5. Polarization curves of individual contributive terms calculated using performance equations for case of Fig. 4. (A) $A_a i_a^0 = 1.4 \times 10^4\,\mathrm{A\,cm^{-3}}$; (B) $A_a i_a^0 = 1.4 \times 10^6\,\mathrm{A\,cm^{-3}}$; (●) activation overpotential; (▲) diffusion overpotential of catalyst layer; (■) diffusion overpotential of gas diffuser.

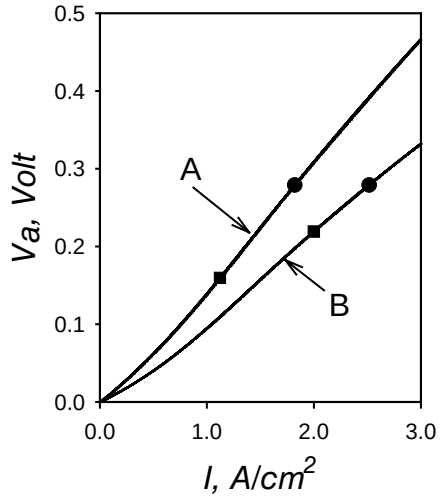

Fig. 7. Polarization curves for anodes with different values of effective proton conductivity of ionomer phase in catalyst layer. (A) $k_a^{eff} = 0.01\,\mathrm{S\,cm^{-1}}$; (B) $k_a^{eff} = 0.1\,\mathrm{S\,cm^{-1}}$; (●) one-dimensional model; (■) performance equations.

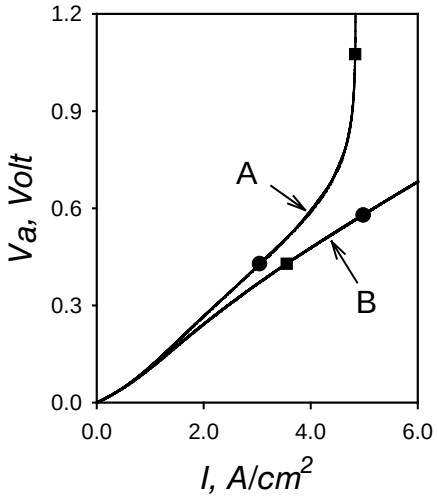

Fig. 8. Polarization curves for anodes with different effective porosity of gas diffuser. (A) $\varepsilon_a = 0.08$; (B) $\varepsilon_a = 0.5$; (●) one-dimensional model; (■) performance equations.

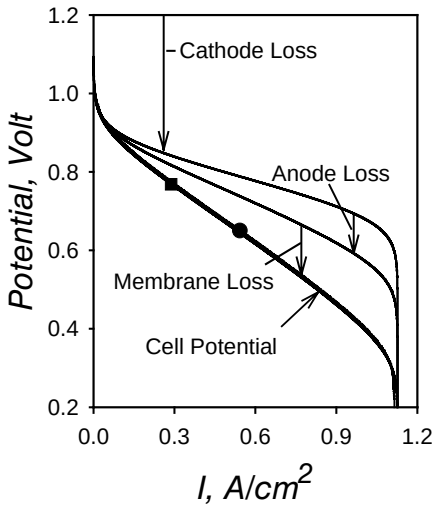

Fig. 9. Potential losses of cathode, anode, membrane electrolyte and single cell for base case (Tables 1 and 2). (●) One-dimensional model; (■) performance equations.

based on these two models nearly overlap. Moreover, the anode with $k_a^{eff} = 0.1\,S\,cm^{-1}$ always demonstrates a better performance than that with $k_a^{eff} = 0.01\,S\,cm^{-1}$ for the same current density. This effect can be quite clearly revealed by Eqs. (27) and (38) since k_a^{eff} only appears in the term involving the ohmic loss caused by proton migration in the performance equations.

Due to relatively large values of gas-pair diffusivity for hydrogen, the influence of the effective porosity of the diffuser on anode performance only appears in the range of high current densities, which are far beyond the values of normal operation. Since the objective of the present study is to examine the accuracy of the performance equations by considering the numerical solutions of the original one-dimensional model as exact ones, it is also interesting to investigate the accuracy of the performance equations in the region near the limiting current. In order to achieve this purpose, a small value of ε_a, namely 0.08, was selected for calculations so as to lower the limiting value of current density. In addition, another ε_a value larger than that in the base case was also chosen for comparisons. The results of both cases are shown in Fig. 8. As seen, the present two models yield almost same values of anode polarization. At low current densities, where diffusion limitations of hydrogen within the diffuser are not significant, the performances of these two anodes are quite close. Nevertheless, as the current density is increased, hydrogen transport resistances within the diffuser play more important roles in anode performance, and thus the anode with $\varepsilon_a = 0.08$ yields a higher potential loss than the one with $\varepsilon_a = 0.5$. It is also noted that ε_a significantly influences the value of the limiting current, which can be exactly calculated by using Eq. (18).

Comparisons between the polarization curves obtained from the performance equations of a complete PEFC and from the corresponding one-dimensional model have been carried out and the results are shown in Fig. 9. The potential losses pertinent to its cathode, anode and membrane electrolyte, calculated using the performance equations, are also illustrated for detailed analysis. The values concerning the physical and chemical properties of the cathode and membrane electrolyte used for the computations are listed in Table 2. The effective porosity of the cathode diffuser

Table 2
Values of physical and chemical parameters for cathode and membrane electrolyte used for calculations

Effective ionic conductivity of ionomer in cathode, k_c^{eff} ($S\,cm^{-1}$)	3×10^{-2}
Effective electric conductivity of cathode gas diffuser, σ_c^{eff} ($S\,cm^{-1}$)	0.5
Effective porosity of cathode gas diffuser, ε_c	0.12
Effective diffusivity of dissolved oxygen in the cathode catalyst layer, $D_{O_2}^{eff}$ ($cm^2\,s^{-1}$)	5×10^{-7}
Effective gas-pair diffusivity, $D_{O_2-N_2}^{eff} (= \varepsilon_c^{1.5} D_{O_2-N_2})$ ($cm^2\,s^{-1}$)	2.32×10^{-3}
Effective gas-pair diffusivity, $D_{N_2-w}^{eff} (= \varepsilon_c^{1.5} D_{N_2-w})$ ($cm^2\,s^{-1}$)	3.22×10^{-3}
Effective gas-pair diffusivity, $D_{O_2-w}^{eff} (= \varepsilon_c^{1.5} D_{O_2-w})$ ($cm^2\,s^{-1}$)	3.08×10^{-3}
Thickness of cathode gas-diffuser, d_c (μm)	300
Thickness of cathode catalyst-layer, δ_c (μm)	10
Product of platinum surface area and reference exchange current density of cathode, $A_c i_c^o$ ($A\,cm^{-3}$)	5×10^{-4}
Cathode pressure, P_c (atm.)	5
Bulk oxygen mole fraction, $x_{O_2}^b$	0.190
Bulk nitrogen mole fraction, $x_{N_2}^b$	0.716
Mole fraction of water vapor in cathode, $x_{w,c}$	0.094
Henry's constant for hydrogen, H_{O_2} (atm. cm^3 per mole)	2×10^5
Equilibrium potential of cathode, V_c^0 (V)	1.2
Cathode transfer coefficient, α_c	0.5
Membrane thickness, δ_m (μm)	125
Ionic conductivity of membrane, k_m ($S\,cm^{-1}$)	0.07

employed for calculations is smaller than its counterpart of the anode so as to account for the effects of water accumulation within the cathode diffuser. As seen, the polarization curves constructed by these two models are well matched. According to the results presented above and in the previous work, at low current densities, a major part of the polarization comes from the activation overpotential for the oxygen reduction reaction. As the current density is increased, overpotentials from other sources such as ohmic losses due to electron conduction and proton migration, diffusion overpotentials of the catalyst layers and the cathode gas-diffuser, play more important roles in cell performance. Bear in mind that the activation overpotential for the hydrogen oxidation reaction is always negligible due to its extremely fast reaction rates. In addition, owing to relatively large values of hydrogen gas-pair diffusivity, the diffusion overpotential of the anode diffuser is also small for the current range calculated. The ohmic loss of membrane is described by Ohm's law, which presents a linear dependence on current density. The polarization curves shown in Fig. 9 reveal these consequences. At low current densities, cathode loss is predominant. As the current density is increased, the anode and membrane losses gain more importance, and substantially engage in the overall cell overpotential. Finally, the limiting value of current density is determined by the mass transport limitations of the cathode diffuser alone. It should be pointed out that it is not necessary to investigate the accuracy of the performance equations for a complete PEFC since its overall potential loss is only a linear addition of individual losses of its anode, cathode and membrane electrolyte. The accuracy of the performance equations for cathode and anode has been investigated in the present and previous studies, in addition, the membrane loss can be estimated exactly because of its linearity. Therefore, a high accuracy of the performance equations for a complete PEFC is concluded for the parameter range investigated.

6. Summary and conclusions

A one-dimensional model has been formulated to take into account the transport and electrochemical processes within the anode catalyst layer and diffuser of PEFCs, and to produce performance equations in algebraic form. The reduction procedures are performed by employing a fourth-degree polynomial approximation or a piecewise one for the hydrogen concentration profile within the catalyst layer contingent upon the occurrence of hydrogen depletion at the interface between the membrane and the anode catalyst-layer. After lumping the reaction rate at a reaction centre, the performance equations in algebraic form are derived. Like the equations for cathodes developed previously, individual overpotential terms, resulting from the limiting processes considered in the original one-dimensional model, can be quantitatively estimated for the anode. Computational results show that the polarization curves created by the anode performance equations and by the one-dimensional model agree well for the extensive parameter range investigated. The performance equations for a complete PEFC are formulated by linearly combining the potential losses pertinent to the cathode, anode and membrane electrolyte. The characteristics of the polarization curves of single cells have been discussed. It is shown that although the anode activation overpotential can be always neglected due to the fast rates of the hydrogen oxidation reaction, other anode potential losses, such as diffusion overpotential of the catalyst layer and ohmic losses caused by proton migration and electron conduction are not negligible at medium and high current densities. Thus, the present performance equations that include the potential losses of the cathode, anode and membrane electrolyte are able to provide accurate evaluation of the performance of a complete PEFC.

Acknowledgements

Financial support from Energy Commission, Ministry of Economic Affairs, Taiwan, ROC (contract no. 92-D0122) is gratefully acknowledged.

References

[1] T. Berning, D.M. Lu, N. Djilali, J. Power Sources 106 (2002) 284.
[2] T.-C. Jen, T. Yan, S.-H. Chan, Int. J. Heat Mass Transfer 46 (2003) 4157.
[3] L. You, H. Liu, Int. J. Heat Mass Transfer 45 (2002) 2277.
[4] S. Um, C.-Y. Wang, K.S. Chen, J. Electrochem. Soc. 147 (2000) 4485.
[5] V. Gurau, H. Liu, S. Kakac, AIChE J. 44 (1998) 2410.
[6] T.F. Fuller, J. Newman, J. Electrochem. Soc. 140 (1993) 1218.
[7] D. Natarajan, T.V. Nguyen, J. Electrochem. Soc. 148 (2001) Al324.
[8] A.A. Kulikovsky, J. Divisek, A.A. Kornyshev, J. Electrochem. Soc. 146 (1999) 3981.
[9] A.C. West, T.F. Fuller, J. Appl. Electrochem. 26 (1996) 557.
[10] W. He, J.S. Yi, T.V. Nguyen, AIChE J. 46 (2000) 2053.
[11] G. Murgia, L. Pisani, M. Valentini, B. D'Aguanno, J. Electrochem. Soc. 149 (2002) A31.
[12] D.M. Bernardi, M. Verbrugge, AIChE J. 37 (1991) 1151.
[13] D.M. Bernardi, M. Verbrugge, J. Electrochem. Soc. 139 (1992) 2477.
[14] C. Marr, X. Li, J. Power Sources 77 (1999) 17.
[15] A. Rowe, X. Li, J. Power Sources 102 (2001) 82.
[16] T.E. Springer, M.S. Wilson, S. Gottesfeld, J. Electrochem. Soc. 140 (1993) 3513.
[17] T.E. Springer, T.A. Zawodzinski, S. Gottesfeld, J. Electrochem. Soc. 138 (1991) 2334.
[18] J.-T. Wang, R.F. Savinell, Electrochim. Acta 37 (1992) 2737.
[19] S. Srinivasan, E.A. Ticianelli, C.R. Derouin, A. Redondo, J. Power Sources 22 (1988) 359.
[20] J. Kim, S.-M. Lee, S. Srinivasan, C.E. Chamberlin, J. Electrochem. Soc. 142 (1995) 2670.
[21] G. Squadrito, G. Maggio, E. Passalacqua, F. Lufrana, A. Patti, J. Appl. Electrochem. 29 (1999) 1449.
[22] J.C. Amphlett, R.M. Baumert, R.F. Mann, B.A. Peppley, P.R. Roberge, T.J. Harris, J. Electrochem. Soc. 142 (1995) 1.
[23] J.C. Amphlett, R.M. Baumert, R.F. Mann, B.A. Peppley, P.R. Roberge, T.J. Harris, J. Electrochem. Soc. 142 (1995) 9.

[24] R.F. Mann, J.C. Amphlett, M. Hooper, H.M. Jensen, B.A. Peppley, P.R. Roberge, J. Power Sources 86 (2000) 173.
[25] L. Pisani, G. Murgia, M. Valentini, B. D'Aguanno, J. Power Sources 108 (2002) 192.
[26] M. Eikerling, A.A. Kronyshev, J. Electroanal. Chem. 453 (1998) 89.
[27] H.-K. Hsuen, J. Power Sources 123 (2003) 26.
[28] A.J. Bard, L.R. Faulkner, Electrochemical Methods, Wiley, New York, 1980.
[29] J. Newman, Electrochemical Systems, Prentice-Hall, Englewood Cliffs, NJ, 1973.
[30] C. de Boor, A Practical Guide to Splines, Springer-Verger, New York, USA, 1978.
[31] S. Hirano, J. Kim, S. Srinivasan, Electrochim. Acta 42 (1997) 1587.